Article

Discovery Medicine 2026; 38(205): 609–622
https://doi.org/10.24976/Discov.Med.202638205.50

Breast Tumor-Secreted APOO Promotes Macrophage Polarization Towards the M2 Phenotype via ADCK2

Jingya Wang[1,*], Rong Fu[1], Qi Yan[1], Xuan Zhang[2], Xingjiang Li[3], Mingxiu Kong[1], Kaiqi Zhang[1], Lili Wang[1]

[1]Department of Oncology, The First Affiliated Hospital of Qiqihar Medical University, 161000 Qiqihar, Heilongjiang, China
[2]Information Center, The First Affiliated Hospital of Qiqihar Medical University, 161000 Qiqihar, Heilongjiang, China
[3]Clinicopathological Center, Qiqihar Medical University, 161000 Qiqihar, Heilongjiang, China
*Correspondence: wjy_qqhr@qmu.edu.cn (Jingya Wang)
Submitted: 30 July 2025 Revised: 18 December 2025 Accepted: 14 January 2026 Published: 20 February 2026

Background: Apolipoprotein O (*APOO*) influences the tumor microenvironment and cancer progression, but its role in macrophage regulation in breast cancer (BC) remains unclear. This study aimed to investigate *APOO*'s effect on macrophage polarization and its molecular mechanisms in BC.

Methods: Gene expression data obtained from single-cell RNA sequencing (RNA-seq) and The Cancer Genome Atlas Breast Invasive Carcinoma (TCGA-BRCA) were analyzed to identify key BC-associated genes. Clinical relevance was validated with TCGA patient data. *APOO* was overexpressed in tumor cells and co-cultured with macrophages. M2 polarization was assessed by cluster of differentiation 206 (CD206) flow cytometry and quantitative real-time PCR (qRT-PCR), and the role of aarF domain containing kinase 2 (*ADCK2*) was evaluated by co-culture with *ADCK2* knockdown macrophages.

Results: Our analysis identified anti-müllerian hormone (*AMH*), *APOO*, neurexophilin 4 (*NXPH4*), and vascular endothelial growth factor (*VEGF*) as key differentially expressed genes in BC. Among these, *APOO* was notably upregulated in tumor tissues as well as correlated significantly with poorer clinical outcomes ($p < 0.05$). Immune infiltration analysis indicated that higher *APOO* expression was linked to enhanced macrophage infiltration, with a notable increase in M2-like macrophages. Functional assays demonstrated that *APOO* promotes M2 macrophage polarization via the *ADCK2* signaling pathway ($p < 0.05$).

Conclusions: These findings suggest that *APOO* may serve as both a potential biomarker and a therapeutic target in BC treatment strategies.

Keywords: breast cancer; macrophage polarization; APOO; ADCK2

Introduction

Breast cancer (BC) stands as the most prevalent malignant tumor among women, representing 30% of newly diagnosed cancer cases in females. In 2023, approximately 2.26 million new cases of BC were identified, making it the primary cause of cancer-related deaths in women [1,2]. Progesterone receptor (PR), Estrogen receptor (ER), as well as human epidermal growth factor receptor 2 (HER2) are three key biomarkers for BC. Despite significant advancements in targeted therapies based on hormone receptor and HER2 status, which have improved long-term survival rates for BC, treatment for advanced stages remains a formidable challenge [3,4]. The formation of BC changes the structure or regulation of cell oncogenes under the influence of external factors, leading to uncontrolled cell growth and differentiation, and malignant transformation. On the other hand, the tumor microenvironment (TME) also affects the progression of BC [5].

The TME plays an important role in tumor development and metastasis. It consists of tumor cells, surrounding cells, and the extracellular matrix. Through their interactions, these elements facilitate tumor advancement and the spread of cancer [6]. Tumor-associated macrophage (TAM) is an important component of breast tumor inflammatory infiltration. TAM may play a role in preventing or promoting tumors depending on the polarization of macrophages. Macrophages can exhibit different polarized states in the tumor - either promoting (M2-type) or fighting (M1-type) the tumor [7]. M2-type macrophages have been shown to facilitate tumor growth as well as metastasis by supporting the establishment and maintenance of the TME through mechanisms such as promoting angiogenesis, suppressing immune responses, and fostering tissue remodeling [8,9].

Secreted proteins are essential mediators of cell-cell communication within the TME, and they significantly influence the behavior of stromal cells as well as tumor cells [10]. Tumor cells can secrete a variety of proteins that alter the TME to favor tumor growth and immune evasion [11]. An example is Apolipoprotein O (APOO), a protein consisting of 198 amino acids, including a signal peptide

that is 23 amino acids in length. The gene for apolipoprotein O is expressed in various human tissues. APOO has also been identified in several types of lipoproteins, including low-density lipoprotein (LDL), high-density lipoprotein (HDL), and very-low-density lipoprotein (VLDL). Besides serving as a secretory protein outside the cell, APOO can also remain within the cell, becoming a component of the intracellular membranes, such as lipid droplets and mitochondrial membranes. Multiple studies have demonstrated that APOO is highly expressed in hepatoma cells and plays a role in atherosclerosis [12,13]. Nevertheless, the function of APOO in BC remains unreported.

This study uniquely reveals that APOO, as a factor secreted by BC cells, can directly promote the polarization of macrophages towards an M2-type, which is closely connected with the progression and prognosis of BC. Using a sequence of experiments conducted both *in vitro* and *in vivo*, this research elucidates the molecular mechanisms by which APOO facilitates M2 polarization and demonstrates how this process exacerbates BC by promoting tumor growth and metastasis. These findings not only enhance our understanding of cellular communication mechanisms within the tumor microenvironment but also may provide a potential target for the development of new BC treatment strategies.

Methods

Data Acquisition

RNA sequencing data for BC and normal samples were obtained from The Cancer Genome Atlas Breast Invasive Carcinoma (TCGA-BRCA) dataset via the University of California, Santa Cruz (UCSC) XENA platform (https://xenabrowser.net/datapages/; accessed September 2024, University of California, Santa Cruz, CA, USA), including 1109 tumor and 113 normal tissue samples. This dataset provides RNA-seq profiles, survival information, and clinical characteristics, allowing classification into four molecular subtypes based on ER, PR, and HER2 status: Luminal A, Luminal B, HER2+, and triple-negative BC [14]. Additionally, secretory protein gene data (275 genes) were retrieved from the Human protein Atlas (HPA) database (https://www.proteinatlas.org/; version updated September 2024, Stockholm, Sweden), with data updated through September 2024. Discovery and cross-subtype characterization were conducted using public cohorts. All TCGA-BRCA subtypes were analyzed in order to (i) maximize statistical power, (ii) evaluate both subtype-agnostic and subtype-specific signals, and (iii) provide a rationale for validating key findings in an independent HER2+ clinical cohort.

Single-cell RNA sequencing (scRNA-seq) Analysis

The scRNA-seq data were retrieved from the GEO database (GSE161529, https://www.ncbi.nlm.nih.gov/geo/query/acc.cgi?acc=GSE161529; accessed September 2024, National Center for Biotechnology Information, Bethesda, MD, USA) [15]. Specifically, GSE161529 contains single-cell RNA-seq data from 7 breast invasive carcinoma tissue samples and 7 adjacent non-tumor tissue samples. We used only the primary tumor tissues from this dataset for single-cell analyses [15].

Raw matrices were processed in Seurat (version 4.3.0; Satija Lab, New York, NY, USA). Genes detected in fewer than 3 cells were filtered, and cells were removed if they showed >10% mitochondrial gene content, <300 detected genes, or >30,000 UMIs (to exclude low-quality cells and potential multiplets). Expression values were normalized using NormalizeData. Highly variable genes (n = 2000) were identified with FindVariableFeatures and used for PCA; the top 20 PCs were retained for downstream analyses. Unsupervised clustering employed FindNeighbors and FindClusters (resolution = 0.4), and embeddings were computed with RunUMAP. Cluster marker genes were identified using FindAllMarkers with adjusted $p < 0.01$ and $|\log2FC| > 1$. Cell types were annotated with SingleR (version 1.12.0; Bioconductor, Seattle, WA, USA). To infer intercellular communication, we used CellChat (version 1.6.1; CellChatDB ligand-receptor reference, R package, Satija Lab, New York, NY, USA) [16].

Identification of Key Secretory Genes

Key genes were identified by integrating single-cell, bulk RNA-seq, and survival analyses. Differential expression between malignant and non-malignant epithelial cells in GSE176078 was performed using FindMarkers (adjusted $p < 0.01$, $|\log2FC| > 1$). Bulk tumor–normal differentially expressed genes (DEGs) in TCGA-BRCA were identified with limma ($|\log2FC| > 1$, false discovery rate (FDR) < 0.05). Prognostic relevance was assessed by univariate Cox regression ($p < 0.05$). The final key genes were determined by intersecting the results of all three analyses, retaining only genes that were (i) upregulated in malignant epithelial cells, (ii) significantly dysregulated in bulk tumor tissues, and (iii) associated with survival.

Immune Infiltration Analysis

To thoroughly examine the degree of local immune cell infiltration in BC, we utilized both the “relative” and “absolute” approaches provided by the CIBERSORT (https://cibersort.stanford.edu/; accessed September 2024, Stanford University, Stanford, CA, USA) [17]. These methods enable a comprehensive evaluation of immune cell presence and their relative contributions. We investigated the possible relationship between the validated hub genes and 22 immune-related cell infiltrations. Using the “MCP-counter” R package (version 1.2.0; Gent University, Gent, Belgium), we further investigated the relationship between confirmed hub genes and the levels of immune cells in BC tissue.

Construction of ROC Curve and Nomogram

Multivariate logistic regression analyses were performed on these genes to assess their diagnostic value for predicting BC. Receiver operating characteristic (ROC) curves and the corresponding area under the curve (AUC) values were calculated using the "pROC" R package (version 1.18.0; Xavier Robin, Paris, France), which is specifically designed for ROC analysis. To further facilitate prediction of the likelihood of BC, we constructed a nomogram utilizing the "rms" R package (version 6.7-0; Frank Harrell, Vanderbilt University, Nashville, TN, USA), with the overall score computed as an amalgamation of all predicted values.

Clinical Sample Collection

A total of 20 HER2+ patients were included in the study between May 2023 and December 2023 at the First Affiliated Hospital of Qiqihar Medical University (Qiqihar, China). All procedures were conducted in accordance with the Declaration of Helsinki, and the study was approved by the Institutional Ethics Committee of the First Affiliated Hospital of Qiqihar Medical University (Approval No. 2024-021-01). Written informed consent was obtained from all participants. Inclusion criteria: histologically confirmed HER2-positive breast cancer, age 18–75 years, scheduled for surgical resection, and provision of written informed consent. Exclusion criteria: history of other malignancies, prior neoadjuvant therapy, severe comorbidities or uncontrolled systemic disease, and pregnancy or lactation.

During surgery, tumor and adjacent tissues were collected using a standardized kit containing paraffin embedding containers and preservation tubes, ensuring consistent sample handling for downstream analyses.

Cell Culture and THP-1 Polarization Detection

Michigan Cancer Foundation-7 breast cancer cell line MCF-7 (American Type Culture Collection, ATCC® HTB-22™, #HTB-22) and human acute monocytic leukemia cell line THP-1 (ATCC® TIB-202™, #TIB-202) cells were obtained from the ATCC cell bank. All cell lines were authenticated by short tandem repeat (STR) profiling and regularly tested for mycoplasma contamination using the MycoAlert™ Mycoplasma Detection Kit (Lonza, #LT07-318). Only those cultures that returned negative results were used in subsequent experiments.

THP-1 cells were differentiated into macrophage-like cells by seeding at 1×10^6 cells/mL and treated with 5 ng/mL phorbol 12-myristate 13-acetate (phorbol 12-myristate 13-acetate (PMA), #P8139; Sigma-Aldrich, St. Louis, MO, USA) for 48 hours at 37 °C with 5% CO_2 [18]. Following PMA treatment, cells were rested in fresh Roswell Park Memorial Institute (RPMI)-1640 medium (RPMI-1640, #11875-093; Gibco, Waltham, MA, USA) supplemented with 10% fetal bovine serum (FBS, #10099-141; Gibco,Waltham, MA, USA) for 24 hours to stabilize differentiation.

For the co-cultured assay, MCF-7 cells (1×10^5) were seeded in the upper chamber of Falcon® Cell Culture Inserts, and PMA-differentiated THP-1 macrophages (1×10^5) were placed in the lower chamber. Co-culture was maintained for 48 hours. Control experiments consisted of THP-1 cells cultured with RPMI medium only. After co-culture, THP-1-derived macrophages were harvested to evaluate M2 polarization. The proportion of M2 macrophages was assessed by flow cytometry using CD206 staining, and the expression of M2-associated genes (*CD206*, arginase 1 (*Arg 1*), interleukin 10 (*IL-10*), c-c motif chemokine ligand 8 (*CCL8*)) was quantified by quantitative reverse transcription polymerase chain reaction (qRT-PCR). In certain experiments, macrophages were pretreated with siRNA to knock down aarF domain containingk kinase 2 (*ADCK2*) prior to co-culture, allowing assessment of the APOO-ADCK2 axis in regulating M2 polarization. All cells were maintained at 37 °C in humidified incubator with 5% CO_2.

Immunofluorescence Staining

Frozen sections (8 µm) from BC patient samples were fixed in 4% paraformaldehyde for 15 min, permeabilized with 0.1% Triton X-100 for 10 min, and blocked with 5% bovine serum albumin (BSA) for 1 h at room temperature. Sections were incubated overnight at 4 °C with primary antibodies against APOO (Abcam, ab246865, Cambridge, UK, dilution 1:200) , CD206 (M2 macrophage marker; Abcam, ab64693, 1:100, Cambridge, UK, dilution 1:100), ADCK2 (Proteintech, #20952-1-AP, Rosemont, IL, USA, dilution 1:200), TM9SF3 (proteintech, #17093-1-AP, Rosemont, IL, USA, dilution 1:1000), and ABCB10 (Abcam, ab231535; Cambridge, UK, dilution 1:200).

After washing, sections were incubated with secondary antibodies conjugated to Alexa Fluor 594 (APOO, red; Invitrogen, #A-11037, Waltham, MA, USA, dilution 1:500) and Alexa Fluor 488 (CD206, blue; Invitrogen, A-11001, Waltham, MA, USA, dilution 1:500) for 1 h at room temperature. Nuclei were counterstained with 4′,6-diamidino-2-phenylindole (DAPI, Sigma-Aldrich, #D9542; St. Louis, MO, USA; 1 µg/mL). Single-stained control sections for APOO and CD206 were included to confirm antibody specificity and prevent fluorescence bleed-through. Images were captured using an Axio Observer Inverted Fluorescence Microscope (Zeiss, model: Axio Observer Z1, Oberkochen, Germany). Five non-overlapping images per tumor were acquired for each channel. For quantitative analysis, APOO-positive tumor cells and CD206-positive M2 macrophages were manually counted using ImageJ (version 1.53t; National Institutes of Health, Bethesda, MD, USA). The M2/tumor cell ratio was calculated as the number of M2 macrophages di-

vided by the number of APOO-positive tumor cells in each image. The mean ratio of five images was used to represent each tumor sample. Statistical significance between APOO-high and APOO-low groups was assessed using an unpaired two-tailed Student's *t*-test. Colocalization analysis was performed using ImageJ software with the Coloc2 plugin.

ADCK2 Knockdown by Small Interfering RNA (siRNA)

To assess the role of ADCK2 in macrophage polarization, PMA-differentiated THP-1 cells were transfected with siRNA targeting *ADCK2* or a non-targeting control siRNA (si-NC). Transfections were performed using Lipofectamine RNAiMAX (Thermo Fisher Scientific, #13778030; Waltham, MA, USA) according to the manufacturer's protocol. Briefly, 50 nM siRNA was complexed with Lipofectamine RNAiMAX in Opti-MEM for 10 min at room temperature and then added to differentiated THP-1 cells, which were incubated for 48 h at 37 °C with 5% CO_2. Knockdown efficiency was confirmed by qRT-PCR. This protocol has been widely used for gene silencing in macrophage differentiation models. Full sequences of all siRNAs are provided in **Supplementary Table 1**.

Rescue Experiment

Human THP-1 monocytes were differentiated into macrophages using PMA (100 ng/mL, 48 h), followed by culture in RPMI 1640 medium containing 10% FBS. Macrophages were transduced with lentiviral particles encoding either non-targeting control siRNA (siNC) or *ADCK2*-specific siRNA (siADCK2). Knockdown efficiency was validated by qPCR and western blot. Cells were then transfected with either *APOO* overexpression plasmid (APOO-OE) or empty vector (EV) using Lipofectamine 3000 (Thermo Fisher Scientific, Waltham, MA, USA). Full sequences of all siRNAs and plasmids are provided in **Supplementary Table 1**.

Orthotopic Xenograft Model

Female NOD/SCID mice (6–8 weeks old, 18–20 g, Beijing Vital River Laboratory Animal Technology) were maintained under pathogen-free conditions with ad libitum access to food and water. All animal procedures were approved by the Animal Ethics Committee of the First Affiliated Hospital of Qiqihar Medical University (Approval No. 2025-14) and were conducted in accordance with the Guidelines for the Care and Use of Laboratory Animals.

A total of 24 mice were used in this study and randomly divided into 4 groups (n = 6 per group): APOO overexpression (APOO-OE), APOO knockdown (siAPOO), and the corresponding controls (Vector, siNC). Stable MCF-7 cell lines were generated via lentiviral transduction and puromycin selection. For orthotopic xenografts, 2×10^6 cells suspended in 50 µL Matrigel (BD Biosciences, Franklin Lakes, NJ, USA) were injected into the mammary fat pads of anesthetized mice with 2–3% isoflurane for induction and 1–2% isoflurane for maintenance via inhalation using a calibrated vaporizer. Tumors became palpable within 7–10 days post-injection, and successful modeling was defined as tumors reaching at least 50 mm^3 in volume. Tumor growth was monitored every 3 days by caliper measurement, and tumor volume was calculated as $V = (L \times W^2)/2$, where L is length and W is width. At the study endpoint (4 weeks), mice were euthanized by CO_2 inhalation, and tumors were excised, weighed, and processed for downstream analyses.

qRT-PCR

RNA extraction was carried out by the SV Total RNA Isolation System (Promega, #Z3100, Madison, WI, USA). cDNA synthesis was conducted by the Reverse Transcription System (Promega, #A3500, Madison, WI, USA) for 60 min at 42 °C. qRT-PCR was carried out with the SYBR and Fluorescein Kit (Bio-Rad, #1708882) on an Applied Biosystems QuantStudio 5 Real-Time PCR System (Thermo Fisher Scientific, Waltham, MA, USA). Thermal cycling conditions: initial denaturation at 95 °C for 10 min, followed by 40 cycles of 95 °C for 15 s and 60 °C for 1 min. The $2^{-\Delta\Delta CT}$ method was used to conducted analysis. Glyceraldehyde-3-phosphate dehydrogenase (*GAPDH*) was selected as the internal control due to its stable and consistent expression across different samples and experimental conditions. The primer sequences are listed in Table 1.

Enzyme-Linked Immunosorbent Assay (ELISA) Analysis

Tumor lysates were homogenized in radioimmunoprecipitation assay (RIPA) buffer supplemented with protease inhibitors. Cytokine levels of IL-10, CCL8, transforming growth factor-beta (TGF-β), IL-12, and TNF-α were measured using commercially available ELISA kits (R&D Systems) with the following catalog numbers, IL-10 (Catalog #DY217B), CCL8 (Catalog #DY529-05), TGF-β (Catalog #DY1679), IL-12 (Catalog #DY518), TNF-α (Catalog #DY210-05). Assays were performed according to the manufacturer's instructions, and absorbance was measured at 450 nm using a BioTek Synergy HTX microplate reader (BioTek Instruments, Inc., Model #HTX, Winooski, VT, USA). Cytokine concentrations were calculated from standard curves using a four-parameter logistic regression.

Western Blot Analysis

Tissues and cells were washed in phosphate-buffered saline (PBS) and then lysed with RIPA lysis buffer (50 mM Tris-HCl (pH 7.4), 1% NP-40, 150 mM NaCl, 0.1% sodium dodecyl sulfate (SDS), 1% deoxycholic acid, 1 mM ethylenediaminetetraacetic acid (EDTA) and 10% glycerol) supplemented with a protease and phosphatase inhibitors cocktail table (Roche, # 04693159001, Basel, Switzerland).

Table 1. The primers for qRT-PCR.

GAPDH (homos)	Glyceraldehyde-3-Phosphate Dehydrogenase	Forward	5′-TCAAGGCTGAGAACGGGAAG-3′
		Reverse	5′-CGCCCCACTTGATTTTGGAG-3′
APOO (homos)	Apolipoprotein O	Forward	5′-CCTTCAAAGTCTATGCAGCACC-3′
		Reverse	5′-TTCGATTGACCCTCAGGAACT-3′
CD206 (homos)	Cluster of Differentiation 206 / Mannose Receptor C Type 1	Forward	5′-GCAGAAGGAGTAACCCACCC-3′
		Reverse	5′-TGGCAAATGAAGGCGTTTGG-3′
Arg 1 (homos)	Arginase 1	Forward	5′-TGATGTTGACGGACTGGACC-3′
		Reverse	5′-ATCTAATCCTGAGAGTAGCCCTGT-3′
IL-10 (homos)	Interleukin-10	Forward	5′-GCCAAGCCTTGTCTGAGATGATCC-3′
		Reverse	5′-TTCACATGCGCCTTGATGTCTGG-3′
CCL8 (homos)	C-C Motif Chemokine Ligand 8	Forward	5′-TGGAGAGCTACACAAGAATCACC-3′
		Reverse	5′-TGGTCCAGATGCTTCATGGAA-3′
ADCK2 (homos)	AarF Domain Containing Kinase 2	Forward	5′-TCT CGC AGA CCA GTC GGT TG-3′
		Reverse	5′-GCA ACA CTT TCA CTG CCA CG-3′
TNF-α (homos)	Tumor Necrosis Factor alpha	Forward	5′-ATGGGCTACAGGCTTGTCACTC-3′
		Reverse	5′-CTCTTCTGCCTGCTGCACTTTG-3′
IL-12 (homos)	Interleukin-12	Forward	5′-CCCTTGCCCTCCTAAACCA-3′
		Reverse	5′-CTAAGACACCTGGCAGGTCCA-3′
iNOS (homos)	Inducible Nitric Oxide Synthase	Forward	5′-GAGCTTCTACCTCAAGCTATC-3′
		Reverse	5′-CCTGATGTTGCCATTGTTGGT-3′
CD206 (mus)	Cluster of Differentiation 206 / Mannose Receptor C Type 1	Forward	5′-AAGGTTCGGGATTGTGGAGC-3′
		Reverse	5′-TGTCGTAGTCAGTGGTGGT T-3′
Arg 1 (mus)	Arginase 1	Forward	5′-CGTGTACATTGGCTTGCGAG-3′
		Reverse	5′-GGGTGAATGCTGGGTCCAG-3′
IL-10 (mus)	Interleukin-10	Forward	5′-TAACTGCACCCACTTCCCAG-3′
		Reverse	5′-CCTGGGGCATCACTTCTACC-3′
CCL8 (mus)	C-C Motif Chemokine Ligand 8	Forward	5′-TTTGCCTGCTGCTCATAGCT-3′
		Reverse	5′-TCACTGACCCACTTCTGTGTG-3′
TNF-α (mus)	Tumor Necrosis Factor alpha	Forward	5′-GTGGTTGGTGAGCCTGACTC-3′
		Reverse	5′-ACCACATACTTTTGGAGACTGCA-3′
IL-12 (mus)	Interleukin-12	Forward	5′-TTGTCCCTCCGAACCATACC-3′
		Reverse	5′-GGTCGTCTTGG TCCAGTTGT-3′
iNOS (mus)	Inducible Nitric Oxide Synthase	Forward	5′-AGCCATCATTGGGAGTAGACAA-3′
		Reverse	5′-CCAGCTCCCTCCTTCTCCTT-3′
GAPDH (mus)	Glyceraldehyde-3-Phosphate Dehydrogenase	Forward	5′-GGTGCTGAGTATGTCGTGGA-3′
		Reverse	5′-GGGCTAAGCAGTTGGTGGT-3′

Cell lysates were incubated on ice for 30 minutes and then centrifuged at 12,000 ×g for 15 minutes at 4 °C to collect the supernatant. Protein concentration was measured using a bicinchoninic acid (BCA) assay kit (Thermo Fisher Scientific, #23225, Waltham, MA, USA). Equal amounts of protein (20–30 µg) were separated by sodium dodecyl sulfate polyacrylamide gel electrophoresis (SDS-PAGE) and transferred onto polyvinylidene difluoride (PVDF) membranes (Millipore, #IPVH00010, Burlington, MA, USA). After blocking with 5% non-fat milk in Tween 20 (TBST) for 1 hour at room temperature, the membranes were incubated overnight at 4 °C with primary antibodies: anti-APOO (Abcam, #ab246865, dilution 1:1000, Cambridge, UK; dilution 1:1000), and anti-GAPDH (Cell Signaling Technology, #5174, MA, USA; dilution 1:2000). Following primary antibody incubation, the membranes were washed and incubated with horseradish peroxidase (HRP)-conjugated goat anti-rabbit immunoglobulin G (IgG) (Jackson ImmunoResearch, #111-035-003, West Grove, PA, USA; dilution 1:5000) for 1 hour at room temperature. Protein bands were visualized using an enhanced chemiluminescence system (Bio-Rad) and quantified by ImageJ software.

Co-immunoprecipitation (Co-IP) Assay

Human embryonic kidney 293T (HEK293T) cells were used for the Co-IP experiment because of their high transfection efficiency and suitability for transient expression of exogenous proteins, allowing reliable assessment of protein-protein interactions *in vitro*. The HEK293T cell line used in this study was a laboratory stock that was originally obtained from ATCC (CRL-3216, Manassas, VA, USA). For transparency, the specific experimental batch employed in these experiments was authenticated by STR profiling and confirmed to be mycoplasma-free prior to use. Cells were maintained under aseptic culture conditions and routinely monitored by microscopy.

293T cells were seeded in 6-well plates and transfected with plasmids encoding APOO-Flag and/or ADCK2-HA using Lipofectamine 3000 (Thermo Fisher Scientific, Cat# L3000015, Waltham, MA, USA) according to the manufacturer's instructions. The experimental groups included: APOO-Flag + ADCK2-HA, APOO-Flag + empty vector, empty vector + ADCK2-HA, and IgG control. After 48 hours, cells were harvested and lysed in ice-cold NP-40 lysis buffer (50 mM Tris-HCl, pH 7.4; 150 mM NaCl; 1% NP-40; 1 mM EDTA; protease inhibitor cocktail, Roche, Cat# 11836170001) for 30 minutes.

Cell lysates were centrifuged at 12,000 ×g for 15 minutes at 4 °C to remove debris. For immunoprecipitation, 500 µg of protein was incubated with 2 µg of anti-Flag antibody (Sigma-Aldrich, Cat# F1804, St. Louis, MO, USA) or control IgG (Cell Signaling Technology, Cat# 2729S, Danvers, MA, USA) overnight at 4 °C with gentle rotation, followed by incubation with Protein A/G magnetic beads (Santa Cruz Biotechnology, Cat# sc-2003, Dallas, TX, USA) for 2 hours at 4 °C. The beads were washed three times with lysis buffer, and bound proteins were eluted by boiling in 2× SDS sample buffer for 5 minutes.

Eluted proteins were separated by SDS-PAGE and transferred to the PVDF membranes (Millipore, Cat# IPVH00010). These membranes were probed with anti-HA antibody (Cell Signaling Technology, Cat# 3724S) to detect ADCK2-HA and anti-Flag antibody (Sigma-Aldrich, Cat# F1804) to confirm APOO-Flag expression. Input lysates were analyzed to assess protein expression levels, and IgG IP served as a negative control. Immunoreactive proteins were detected by enhanced chemiluminescence (ECL, Thermo Fisher Scientific, Cat# 32106).

Flow Cytometry

THP-1-derived macrophages were harvested at a density of 1×10^6 cells/mL, washed twice in PBS and incubated with PE-conjugated anti-CD206 antibody (1:50; BioLegend, #321106) for 30 min at 4 °C in the dark. After an additional wash, cells were acquired on a FACSCalibur Flow Cytometer (Becton Dickinson, Model FACSCalibur, Franklin Lakes, NJ, USA) and analysed using FlowJo (BD Biosciences, Version 10.8.1, Ashland, OR, USA). CD206 expression was quantified as the proportion of PE-positive cells within the macrophage gate. APOO-positive tumour cells and CD206-positive M2 macrophages were manually enumerated in five non-overlapping fields per section using ImageJ. The M2/tumour-cell ratio was calculated for each field, and the mean value was used to represent each sample.

Statistical Analysis

Statistical analyses were performed using GraphPad Prism (GraphPad Software, Version 9.5.1, San Diego, CA, USA). Data are presented as mean ± SD from at least three independent experiments. For continuous variables, comparisons between two groups were conducted using the unpaired two-tailed Student's *t*-test. For comparisons among three or more groups, one-way ANOVA followed by Tukey's multiple comparison test was applied. For categorical variables (e.g., clinical characteristics between groups), Fisher's exact test was used when the expected cell count was <5, and the Chi-square (χ^2) test was used otherwise. A p value < 0.05 was considered statistically significant.

Results

Identification of Secreted Protein-Related Genes Differentially Expressed in BC

Utilizing the HPA database, we obtained genes encoding secretory proteins. These were then cross-referenced with differentially expressed genes in single-cell tumor epithelium, TCGA-BRCA tissue, and genes that showed significance in the univariate Cox regression (Fig. 1B,C). This approach yielded four key genes: *AMH*, *APOO*, *NXPH4*, and *VEGF* (Fig. 1D). The association between *APOO* and BC has not yet been reported, therefore, we selected APOO for subsequent studies. Univariate Cox regression analysis was performed using TCGA-BRCA patient survival data to evaluate the association between the expression of these four secretory protein-related genes and overall survival. The analysis revealed that *APOO*, *AMH*, *NXPH4*, and *VEGF* expression levels were significantly associated with patient prognosis, suggesting their potential value as prognostic biomarkers in BC (Fig. 1E). A flowchart of the analyses is shown in Fig. 1A.

High Expression of APOO in BC

Analysis of the TCGA database revealed that *APOO* is highly expressed in BC tissues ($p < 0.05$, Fig. 2A). To validate these bioinformatics findings, we collected tumor samples from 20 $HER2^+$ BC patients. Based on the median APOO expression level, samples were divided into a high-expression group (n = 10) and a low-expression group (n = 10). qRT-PCR analysis revealed that *APOO* mRNA in BC tissues was approximately 2-fold higher than that in paired adjacent normal tissues ($p < 0.05$, Fig. 2B). ELISA and immunofluorescence analyses further demon-

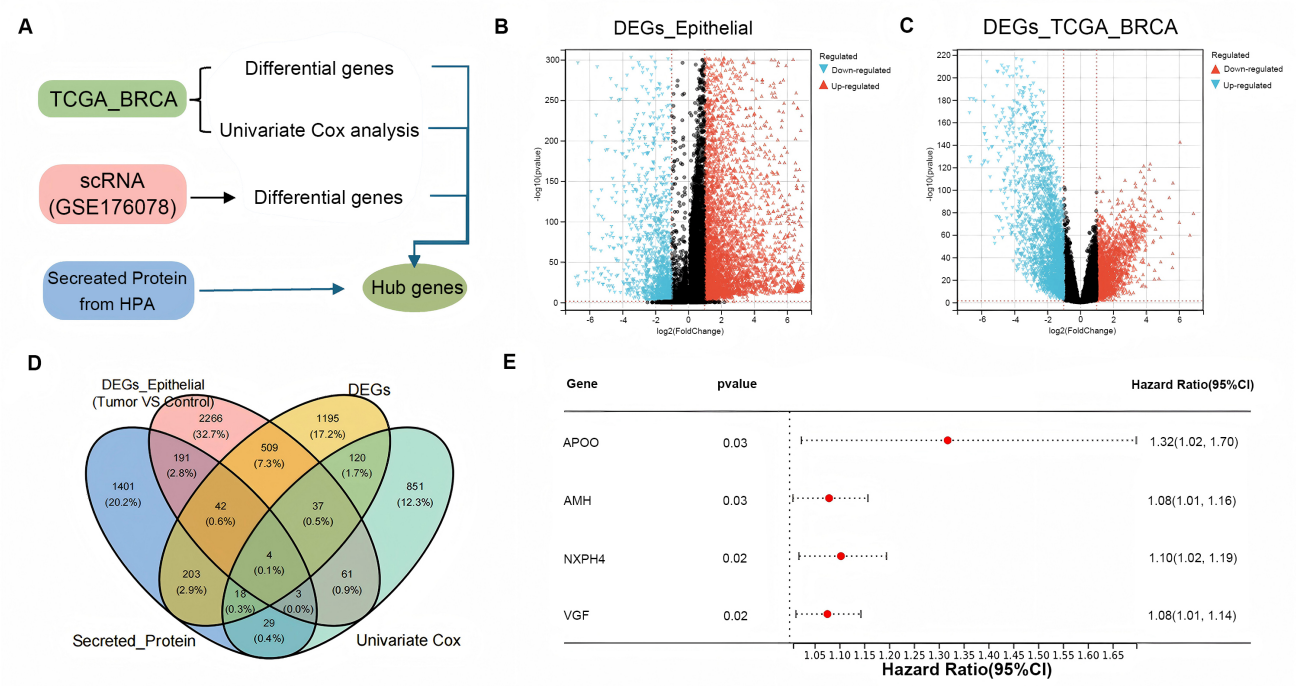

Fig. 1. Identification of secreted protein-related genes differentially expressed in breast cancer (BC). (A) A flowchart of these analyses. (B) Volcano plot of scRNA dataset analysis. (C) Volcano plot of TCGA-BRCA dataset analysis. (D) A Venn diagram of results from analyzing secreted proteins, DEGs epithelial, DEGs and univariate Cox regression. (E) Forest plot of the results from a Cox regression analysis.

strated that APOO is predominantly localized within BC cells, exhibiting consistently elevated expression in the high-expression group compared with the low-expression group and normal tissues ($p < 0.05$, Fig. 2C). Further analysis of scRNA dataset demonstrated that *APOO* is predominantly expressed in epithelial cells (Fig. 2D), with higher expression in tumor epithelia than in precancerous epithelia (Fig. 2E). To verify the secretory nature of APOO and characterize its expression pattern, we cultured commercially available BC cell lines (MCF-7). We analyzed both the supernatant and the cells themselves, and found that APOO expression was elevated both intracellularly, and in the supernatant, compared to normal breast epithelial cells ($p < 0.05$, Fig. 2F). Collectively, these results consistently indicate that APOO is significantly overexpressed in BC tissues and cells.

APOO Is Linked to Immune Cell Infiltration in BC

To investigate the relationship between APOO expression and immune cell infiltration, we analyzed bulk and single-cell transcriptome datasets, which revealed that APOO-high tumors exhibited a significantly higher proportion of M2-type macrophages ($p < 0.05$, Fig. 3A–C).

APOO Encourages Macrophages to Shift Towards the M2 Phenotype In BC Microenvironment

To investigate the effect of tumor-secreted APOO on macrophage polarization, we overexpressed APOO in MCF-7 breast cancer cells and co-cultured them with THP-1 macrophages. Flow cytometry revealed an approximately 2-fold increase in the polarization of macrophages towards the M2 phenotype compared with controls ($p < 0.05$, Fig. 4A,B). Consistently, qRT-PCR analysis demonstrated elevated expression of M2-associated markers, including *CD206*, *CCL8*, *IL-10* and *Arg 1*, in THP-1 cells co-cultured with MCF-7, showing a 1.5–2-fold increase relative to controls ($p < 0.05$, Fig. 4C–F). These results suggest that APOO, when released by tumor cells, promotes macrophage polarization towards the M2 phenotype, underscoring its critical role in shaping the tumor microenvironment.

To validate the functional rescue experiment, we first confirmed APOO overexpression efficiency in THP-1 macrophages by qPCR. APOO overexpression was then performed in ADCK2 knockdown macrophages, and APOO expression remained robust, ensuring the validity of the rescue experiment. To further confirm the specificity of ADCK2 in mediating APOO-induced macrophage polarization, we conducted another functional rescue experiment. THP-1 macrophages were transduced with either siNC or *ADCK2*-targeting siRNA, followed by *APOO* over-

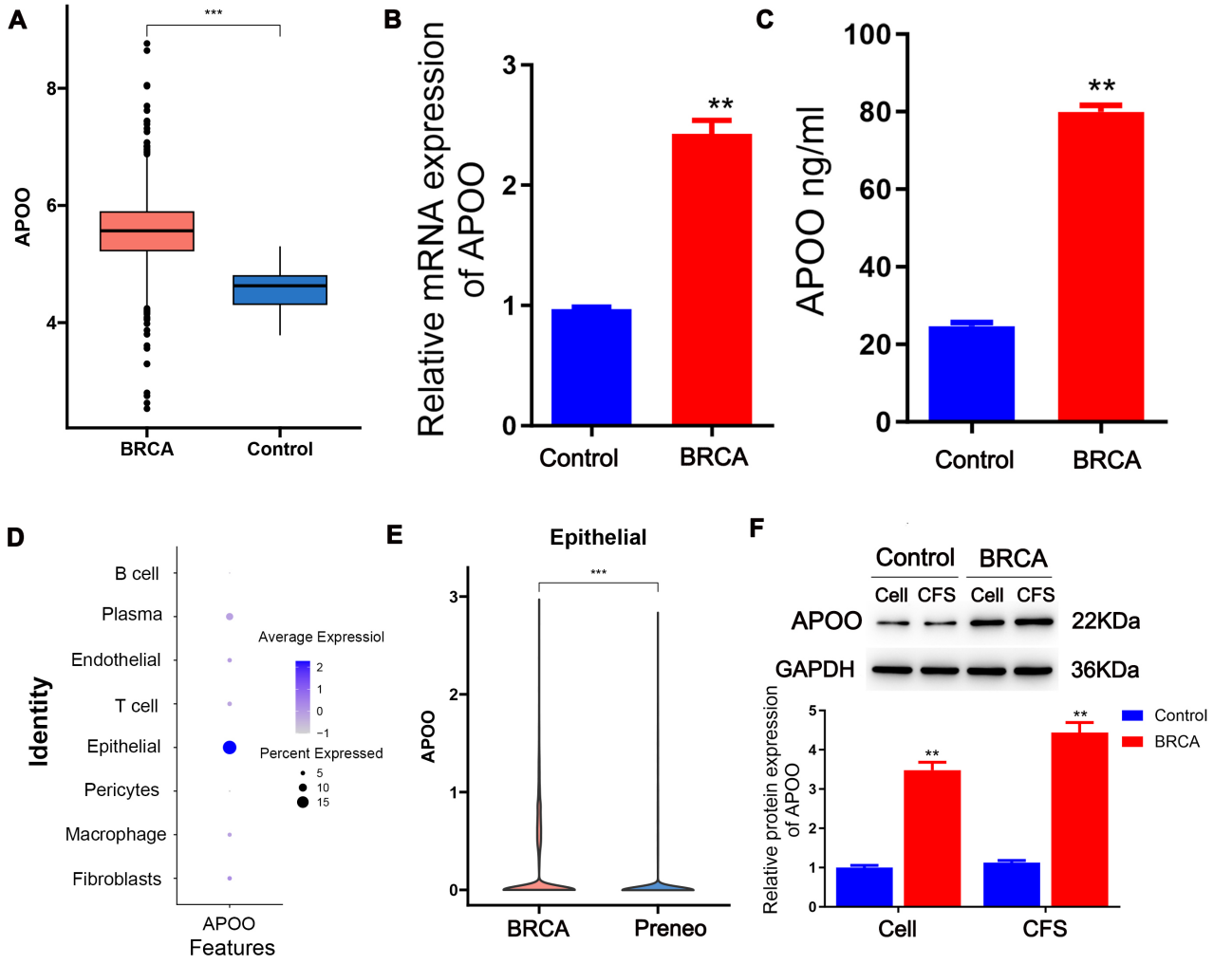

Fig. 2. High Expression of APOO in Breast Cancer Tissues and MCF-7 Cells. High expression of APOO in BC (A) The expression of APOO in BRCA. (B) The relative mRNA of *APOO* in BC tissues (n = 10). (C) The relative figure and intensity of APOO in patients' tumor tissues (n = 10). (D) The expression of APOO in BC single cell datasets. Color indicates scaled average expression (light purple to dark blue), and dot size represents the percentage of expressing cells. (E,F) The protein levels of APOO in supernatant and cell of MCF-7 cells (n = 3). $^{**}p < 0.01$. $^{***}p < 0.001$.

expression. qPCR analysis revealed that *APOO* overexpression upregulated M2 markers (*CD206*, *Arg 1*, *IL-10*, *CCL8*) and suppressed M1 markers (*TNF-α*, *IL-12*, *iNOS*). In contrast, ADCK2 knockdown impaired M2 marker induction and enhanced M1 marker expression, preventing APOO from rescuing M2 polarization ($p < 0.05$, **Supplementary Fig. 1**). These findings confirm that ADCK2 is required for APOO-driven macrophage polarization.

Tumor-Secreted APOO Promotes Macrophage Polarization Towards the M2 Phenotype via ADCK2

To elucidate the molecular mechanism by which APOO promotes M2 polarization, we first examined the expression of candidate interacting proteins (TM9SF3, ABCB10, and ADCK2) in macrophages using single-cell transcriptome data. ADCK2, TM9SF3, and ABCB10 were highly expressed in tumor-associated macrophages compared with precancerous lesions ($p < 0.05$, Fig. 5A,B). Utilizing a transwell coculture system with BC cells and macrophages, we determined that, although TM9SF3-a membrane protein showed strong membrane staining, ADCK2 exhibited significant upregulation on the macrophage membrane under coculture conditions, as confirmed by immunofluorescence ($p < 0.05$, Fig. 5C). To investigate the role of APOO in macrophage polarization through ADCK2, we conducted co-cultures of BC cells overexpressing APOO with macrophages where ADCK2 expression was reduced. *ADCK2* knockdown in macrophages was achieved using siRNA, and the efficiency was confirmed by quantitative PCR ($p < 0.05$, **Supplementary Fig. 2**). The results indicated that decreasing ADCK2 expression can inhibit the polarization effects induced by *APOO* overexpression in macrophages ($p < 0.05$, Fig. 5D). Finally, Co-IP in 293T cells overexpressing

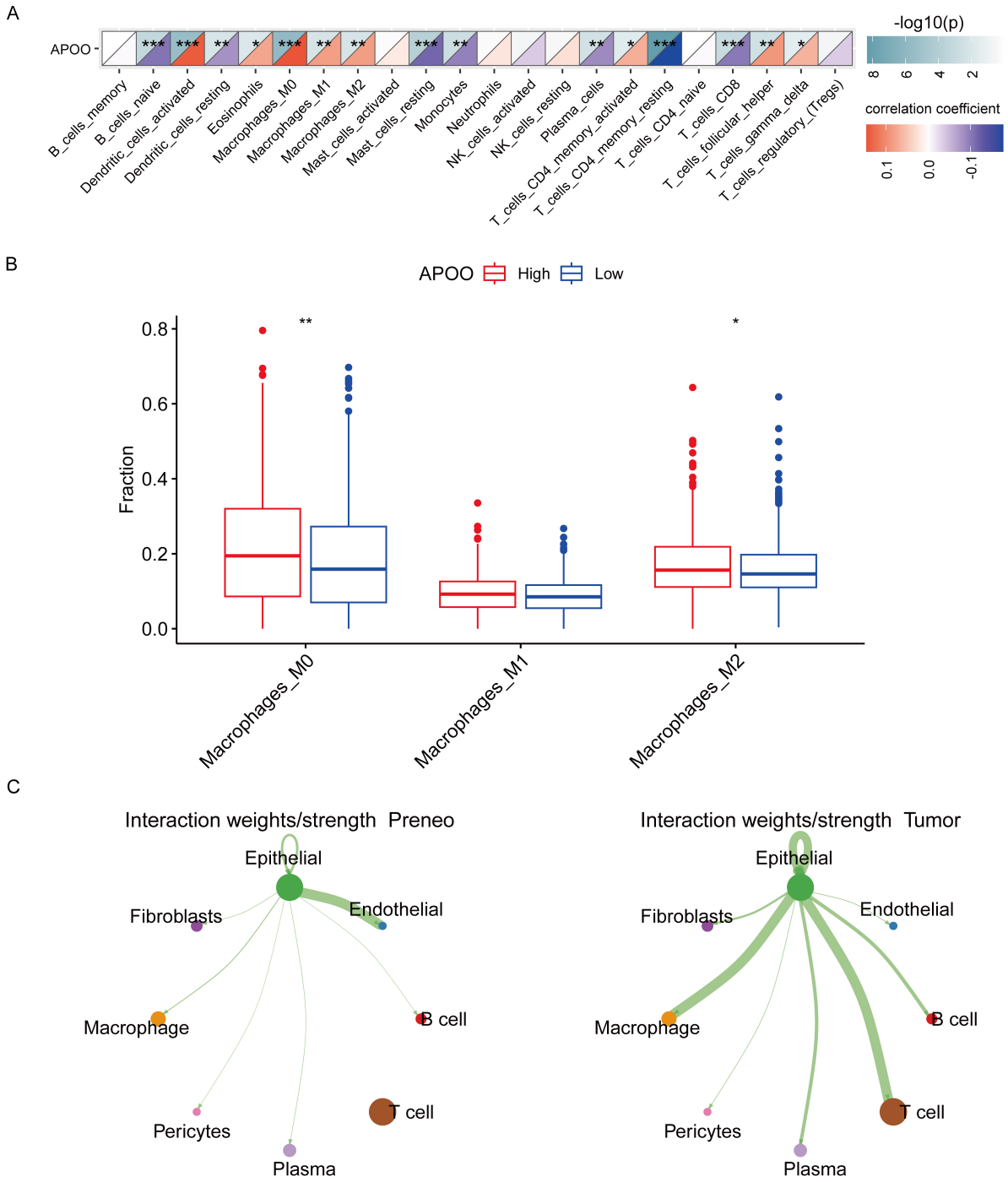

Fig. 3. APOO expression correlates with macrophage infiltration and enhances epithelial-macrophage communication in BC. (A) *APOO* is linked to immune cell infiltration in BC. (B) Single-cell RNA-seq analysis confirming enrichment of M2 macrophages in *APOO*-high tumor tissues. (C) CellChat network plots showing cell–cell communication patterns in preneoplastic and tumor tissues. Node size represents the total number of interactions for each cell type, edge width indicates interaction strength, and arrow direction shows the signaling flow from sender to receiver. $*p < 0.05$, $**p < 0.01$, $***p < 0.001$.

tagged APOO-Flag and ADCK2-HA demonstrated a direct physical interaction between APOO and ADCK2. APOO-Flag successfully pulled down ADCK2-HA, while negative controls (APOO-Flag + Vector, Vector + ADCK2-HA, IgG) showed no signal. Input controls confirmed protein expression (Fig. 5E). Together, these results demonstrate

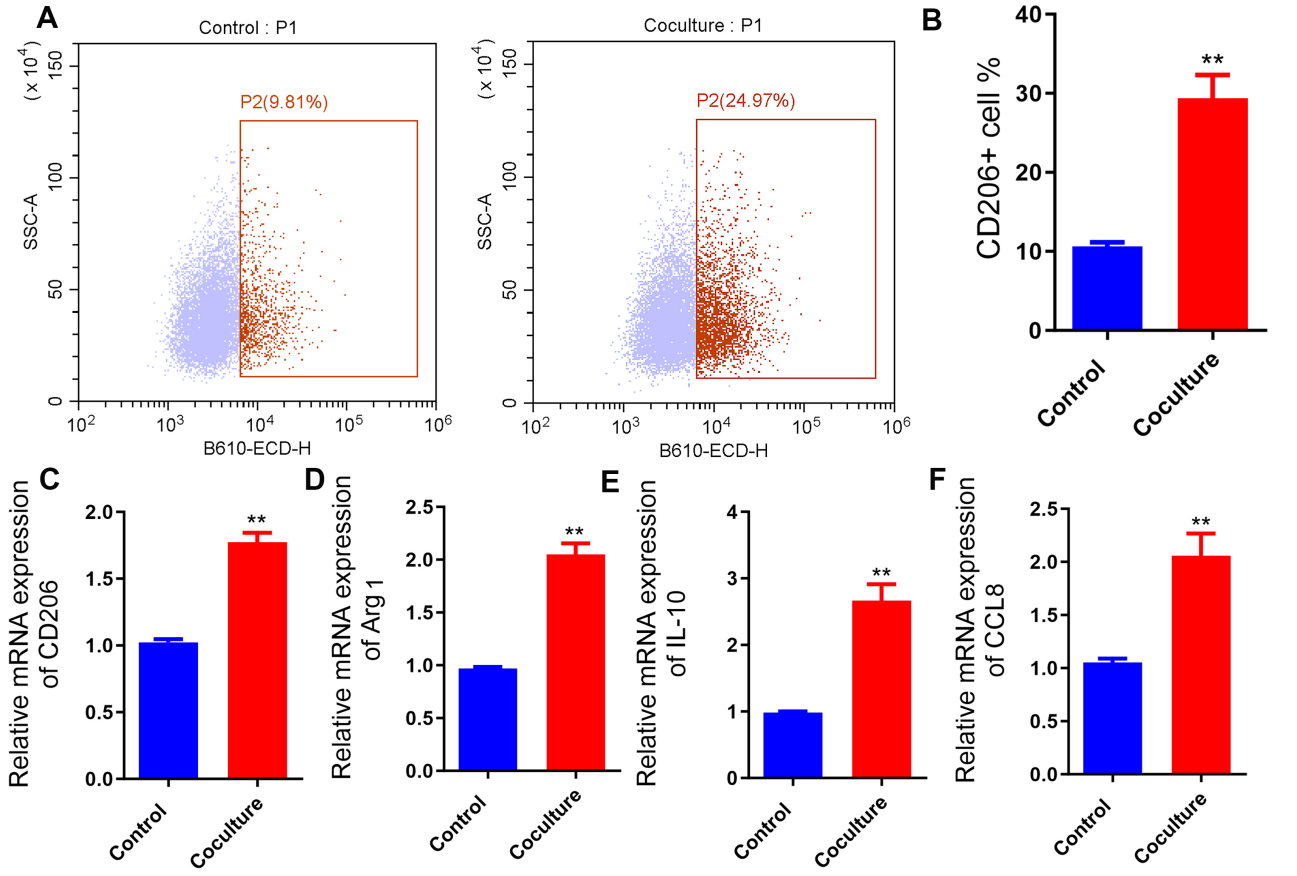

Fig. 4. APOO encourages macrophages to shift towards the M2 phenotype in BC microenvironment. (A) The representative results of CD206-positive cell flow cytometry. (B) The quantification results of percentage of M2 macrophage (n = 3). The mRNA of *CD206* (C), *Arg 1* (D), *IL-10* (E), *CCL8* (F) (n = 3), $^{**}p < 0.01$.

that APOO modulates macrophage polarization by interacting with ADCK2 in the BC microenvironment, establishing the APOO-ADCK2 axis as a critical regulator of M2 macrophage differentiation.

APOO Promotes Tumor Growth and M2 Macrophage Polarization In Vivo

To investigate the role of APOO in breast cancer, we established orthotopic xenograft models using MCF-7 cells with stable *APOO* knockdown or overexpression in female NOD/SCID mice. Tumor growth curves demonstrated that *APOO*-overexpression significantly accelerated tumor progression, while *APOO* knockdown markedly suppressed tumor growth ($p < 0.05$, Fig. 6A). Endpoint tumor weight measurements corroborated these findings ($p < 0.05$, Fig. 6B), providing robust quantitative evidence of APOO's effect on tumor proliferation. Molecular analyses revealed that APOO markedly influenced macrophage polarization *in vivo*. qRT-PCR revealed that tumors with *APOO* overexpression exhibited elevated levels of M2-associated markers (*CD206*, *Arg 1*, *IL-10*, and *CCL8*) alongside reduced expression of M1-associated markers (*TNF-α*, *IL-12*, *iNOS*), whereas *APOO*-knockdown tumors displayed the opposite pattern ($p < 0.05$, Fig. 6C). Consistently, ELISA analysis of tumor lysates confirmed these cytokine alterations at the protein level, IL-10, CCL8, and TGF-β were significantly enriched in *APOO*-overexpression tumors, while proinflammatory cytokines IL-12 and TNF-α were increased in the *APOO*-knockdown tumors ($p < 0.05$, Fig. 6D). Collectively, these results demonstrate that APOO not only accelerates tumor growth but also shapes the tumor immune microenvironment by driving macrophage polarization towards an immunosuppressive M2 phenotype, highlighting its potential as a therapeutic target.

Discussion

Secreted factors from primary tumors significantly influence the tumor microenvironment by modifying the tumor's own secretome via autocrine and paracrine mechanisms [19]. These factors include a diverse array of proteins that can promote chemoresistance, facilitate metastasis, and modulate immune responses [20]. Central to our study is the application of bioinformatics techniques to identify key

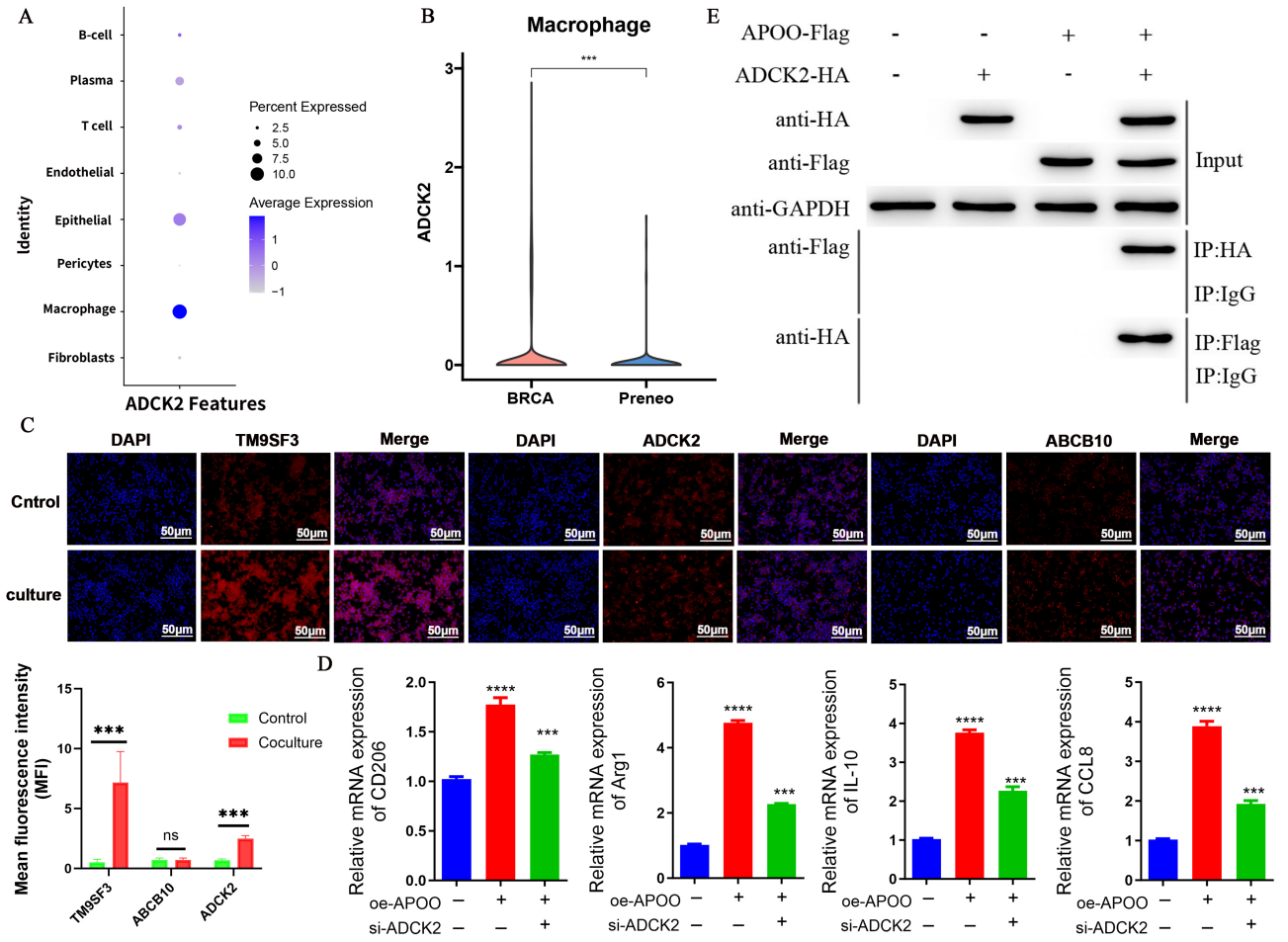

Fig. 5. Tumor-secreted APOO facilitates macrophage polarization towards M2 through ADCK2. (A,B) The expression level of ADCK2, TM9SF3 and ABCB10 in BC single cell datasets. (C) The intensity of ADCK2, TM9SF3 and ABCB10 in THP-1 cocultured with MCF-7. Bar = 50 μm. (D) The mRNA of *CD206*, *Arg 1*, *IL-10*, *CCL8* in THP-1 cocultured with MCF-7 (n = 3). (E) Co-immunoprecipitation (Co-IP) showing the direct physical interaction between APOO and ADCK2. ***$p < 0.001$. ****$p < 0.0001$, ns: no significance.

genes, such as *AMH*, *APOO*, *NXPH4*, and *VEGF*. These genes exhibit unique expression profiles within the single-cell tumor epithelium. Notably, *AMH*, commonly known as a marker for ovarian reserve, correlates positively with increased BC risk [21]. Both *NXPH4* and *VEGF* are linked to prognostic outcomes in BC, highlighting their potential as predictive markers [22,23]. However, the specific role of APOO, a tumor-secreted protein, in BC remains to be elucidated.

APOs are crucial in regulating lipid levels within our bloodstream. Recent advancements in scientific research have revealed a compelling connection between APOs and various types of cancers. Our results reveal that APOO is upregulated in BC and correlates with adverse clinical outcomes, marking it as a significant factor in the disease's pathology. The elevated expression of APOO in liver cancer tumor tissue, as previously reported, is strongly associated with poorer prognosis and more advanced stages of the disease [12]. Additionally, the relationship between APOO expression levels and clinical parameters highlights its possible role as a biomarker for tracking disease progression and categorizing patients, thereby enhancing the precision of treatment planning.

At present, there are relatively few studies on the role of APOO as a secreted protein. This study focused on the relationship between APOO and macrophage polarization to clarify its role in BC. Immune infiltrate analysis uncovered a significant correlation between APOO expression and the presence of macrophages, particularly M2-like macrophages, which are known to support tumorigenesis in various cancers [24]. *In vitro* experiments further corroborated that APOO may enhance the polarization of macrophages toward this pro-tumorigenic M2 phenotype. A novel aspect of our research is the identification of ADCK2 as a mediator in this process, delineating a specific signaling pathway by which APOO influences immune

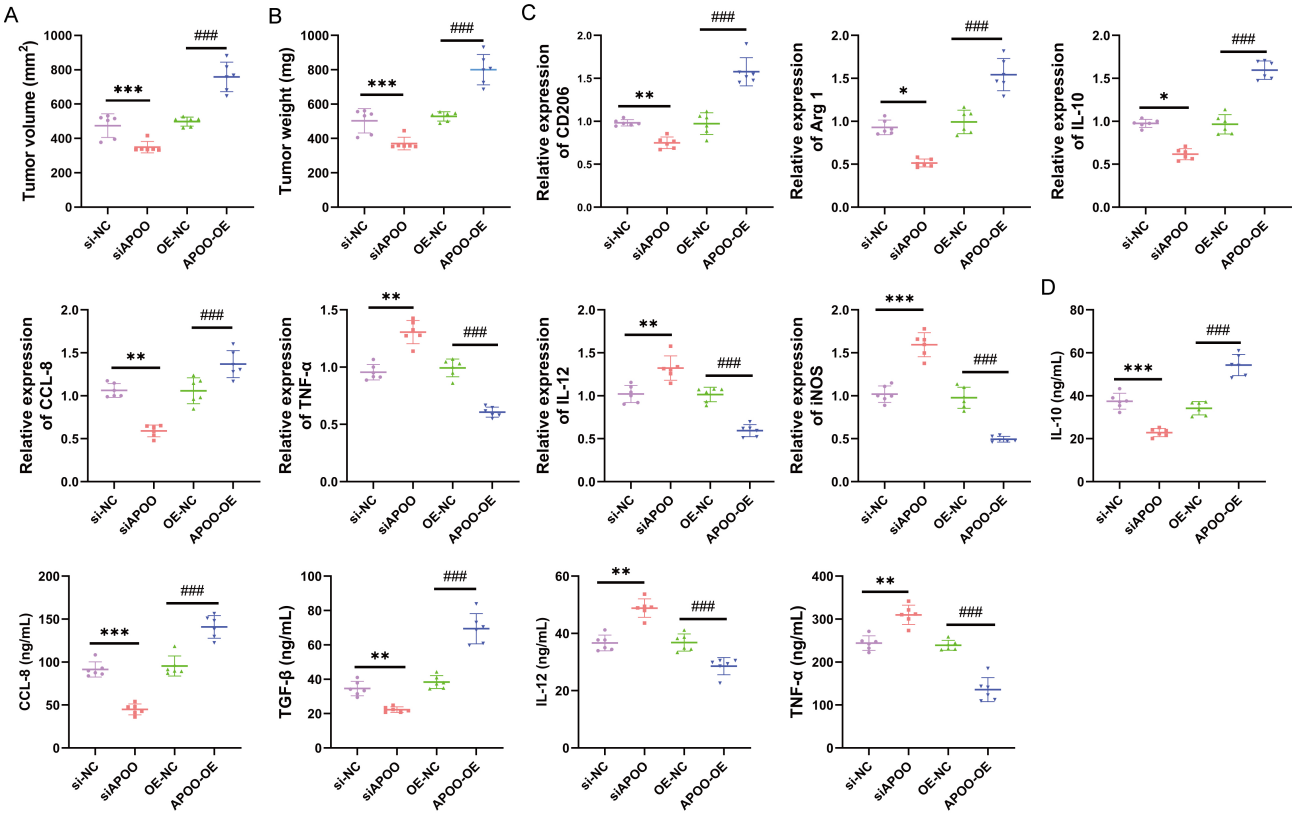

Fig. 6. APOO promotes breast cancer progression and M2 macrophage polarization *in vivo*. (A) Tumor growth curves of orthotopic xenografts derived from MCF-7 cells stably transduced with *APOO*-overexpression (*APOO*-OE), knockdown (si*APOO*), or respective controls (Vector, siNC) (n = 6). (B) Quantification of tumor weights at endpoint. (C) Relative mRNA levels of M2 markers (*CD206*, *Arg 1*, *IL-10*, *CCL8*) and M1 markers (*TNF-α*, *IL-12*, *iNOS*) in xenograft tumors as determined by qRT-PCR (n = 3). (D) ELISA quantification of secreted cytokines in tumor lysates, including IL-10, CCL8, TGF-*β*, IL-12, and TNF-*α* (n = 3). Data are presented as mean ± SD. **p* < 0.05, ***p* < 0.01, ****p* < 0.001, ###*p* < 0.001.

cells in the tumor microenvironment [25]. ADCK2 belongs to the AarF domain-containing kinase family, a group that comprises five members, and is known to be involved in CoQ metabolism and mitochondrial bioenergetics [25,26]. Beyond its metabolic roles, emerging evidence suggests that ADCK2 can modulate key oncogenic signaling pathways, including PI3K/AKT, NF-κB, and STAT3, which are well recognized regulators of macrophage polarization and tumor progression [27]. In this context, APOO binding to ADCK2 may trigger downstream activation of these pathways in macrophages, promoting M2-like polarization, anti-inflammatory cytokine secretion, and suppression of M1-associated responses. Moreover, the APOO-ADCK2 axis may influence the expression of chemokines such as CCL8 and IL-10, thereby enhancing recruitment and maintenance of immunosuppressive macrophages within the tumor microenvironment. These findings suggest that ADCK2 not only supports cancer cell viability and proliferation, as observed in ER+ BC and glioblastoma cells, but also functions as a key node linking tumor-secreted APOO to the reprogramming of the immune microenvironment, highlighting its potential as a therapeutic target [28]. Collectively, these findings indicate the dual role of APOO in BC: (1) Tumor-intrinsic role-APOO promotes cancer cell proliferation, survival, and progression through metabolic and signaling pathways, such as those involving ADCK2. (2) Tumor-extrinsic (immune-modulatory) role-APOO shapes the tumor microenvironment by promoting macrophage polarization toward the M2 phenotype, thereby fostering an immunosuppressive milieu conducive to tumor growth. This dual functionality underscores APOO's complex contribution to BC pathology, integrating both direct effects on tumor cells and indirect effects via immune modulation. Consequently, APOO emerges as a multifaceted and promising target for therapeutic intervention, where blocking its activity could simultaneously impair tumor cell viability and reprogram the immune microenvironment toward anti-tumor responses.

Overall, our study employs advanced bioinformatics and thorough molecular analyses to establish APOO as a pivotal mediator in BC progression, specifically through its role in macrophage polarization. This insight significantly

advances our understanding of the biological mechanisms underpinning BC and introduces APOO as both a potential biomarker and therapeutic target. These findings hold the promise of revolutionizing BC management by facilitating more targeted and effective treatment approaches. Furthermore, the precise receptors and signaling pathways through which APOO influences macrophage behavior require further exploration. We are optimistic that ongoing research and collaborative efforts will further delineate these molecular mechanisms, paving the way for innovative therapeutic strategies and ultimately enhancing patient outcomes in BC.

Conclusion

This study greatly advances our understanding of the biological mechanisms of BC. It found that tumor-secreted APOO promotes the polarization of macrophages towards M2 phenotypes via ADCK2, and identified APOO as a potential biomarker and therapeutic target.

Availability of Data and Materials

The data that support the findings of this study are available from the corresponding author upon reasonable request.

Author Contributions

JYW designed the research study. RF, XJL, MXK and KQZ performed the research. QY and LLW collected the data. XZ and XJL analyzed the data. All authors contributed to drafting the original manuscript and revising it critically for important intellectual content. All authors reviewed and agreed on the final manuscript to be published. All authors have participated sufficiently in the work to take public responsibility for appropriate portions of the content and agreed to be accountable for all aspects of the work in ensuring that questions related to its accuracy or integrity.

Ethics Approval and Consent to Participate

The study was approved by the Ethics Committee of the First Affiliated Hospital of Qiqihar Medical University (Approval No. 2024-021-01) for human subjects and by the Animal Ethics Committee of the First Affiliated Hospital of Qiqihar Medical University (Approval No. 2025-14) for animal experiments. Written informed consent was obtained from all participating patients prior to sample collection. All procedures involving human participants were conducted in accordance with the Declaration of Helsinki.

Acknowledgment

Not applicable.

Funding

This study was funded by Qiqihar City Joint Guidance Project for Science and Technology Planning (LSFGG-2024092).

Conflict of Interest

The authors declare no conflict of interest.

Supplementary Material

Supplementary material associated with this article can be found, in the online version, at https://doi.org/10.24976/Discov.Med.202638205.50.

References

[1] Barzaman K, Karami J, Zarei Z, Hosseinzadeh A, Kazemi MH, Moradi-Kalbolandi S, *et al*. Breast cancer: Biology, biomarkers, and treatments. International Immunopharmacology. 2020; 84: 106535. https://doi.org/10.1016/j.intimp.2020.106535.

[2] Burstein HJ, Curigliano G, Thürlimann B, Weber WP, Poortmans P, Regan MM, *et al*. Customizing local and systemic therapies for women with early breast cancer: the St. Gallen International Consensus Guidelines for treatment of early breast cancer 2021. Annals of Oncology: Official Journal of the European Society for Medical Oncology. 2021; 32: 1216–1235. https://doi.org/10.1016/j.annonc.2021.06.023.

[3] Jallah JK, Dweh TJ, Anjankar A, Palma O. A Review of the Advancements in Targeted Therapies for Breast Cancer. Cureus. 2023; 15: e47847. https://doi.org/10.7759/cureus.47847.

[4] Cao Y, Li Y, Liu R, Zhou J, Wang K. Preclinical and Basic Research Strategies for Overcoming Resistance to Targeted Therapies in HER2-Positive Breast Cancer. Cancers. 2023; 15: 2568. https://doi.org/10.3390/cancers15092568.

[5] Xiao Y, Yu D. Tumor microenvironment as a therapeutic target in cancer. Pharmacology & Therapeutics. 2021; 221: 107753. https://doi.org/10.1016/j.pharmthera.2020.107753.

[6] Elhanani O, Ben-Uri R, Keren L. Spatial profiling technologies illuminate the tumor microenvironment. Cancer Cell. 2023; 41: 404–420. https://doi.org/10.1016/j.ccell.2023.01.010.

[7] Vitale I, Manic G, Coussens LM, Kroemer G, Galluzzi L. Macrophages and Metabolism in the Tumor Microenvironment. Cell Metabolism. 2019; 30: 36–50. https://doi.org/10.1016/j.cmet.2019.06.001.

[8] Yunna C, Mengru H, Lei W, Weidong C. Macrophage M1/M2 polarization. European Journal of Pharmacology. 2020; 877: 173090. https://doi.org/10.1016/j.ejphar.2020.173090.

[9] Boutilier AJ, Elsawa SF. Macrophage Polarization States in the Tumor Microenvironment. International Journal of Molecular Sciences. 2021; 22: 6995. https://doi.org/10.3390/ijms22136995.

[10] Zhang N, Hao J, Cai Y, Wang M. Research advances of secretory proteins in malignant tumors. Chinese Journal of Cancer Research = Chung-kuo Yen Cheng Yen Chiu. 2021; 33: 115–132. https://doi.org/10.21147/j.issn.1000-9604.2021.01.12.

[11] Bushweller JH. Targeting transcription factors in cancer - from undruggable to reality. Nature Reviews. Cancer. 2019; 19: 611–624. https://doi.org/10.1038/s41568-019-0196-7.

[12] Weijler AM, Schmidinger B, Kapiotis S, Laggner H, Hermann M. Oleic acid induces the novel apolipoprotein O and reduces mitochondrial membrane potential in chicken and human hep-

atoma cells. Biochimie. 2018; 147: 136–142. https://doi.org/10.1016/j.biochi.2018.02.003.

[13] Kalaivani V, Jaleel A. Apolipoprotein(a), an enigmatic anti-angiogenic glycoprotein in human plasma: A curse or cure? Pharmacological Research. 2020; 158: 104858. https://doi.org/10.1016/j.phrs.2020.104858.

[14] Tomczak K, Czerwińska P, Wiznerowicz M. The Cancer Genome Atlas (TCGA): an immeasurable source of knowledge. Contemporary Oncology (Poznan, Poland). 2015; 19: A68–77. https://doi.org/10.5114/wo.2014.47136.

[15] Wu SZ, Al-Eryani G, Roden DL, Junankar S, Harvey K, Andersson A, *et al*. A single-cell and spatially resolved atlas of human breast cancers. Nature Genetics. 2021; 53: 1334–1347. https://doi.org/10.1038/s41588-021-00911-1.

[16] Guerrero-Juarez CF, Dedhia PH, Jin S, Ruiz-Vega R, Ma D, Liu Y, *et al*. Single-cell analysis reveals fibroblast heterogeneity and myeloid-derived adipocyte progenitors in murine skin wounds. Nature Communications. 2019; 10: 650. https://doi.org/10.1038/s41467-018-08247-x.

[17] Chen B, Khodadoust MS, Liu CL, Newman AM, Alizadeh AA. Profiling Tumor Infiltrating Immune Cells with CIBERSORT. Methods in Molecular Biology (Clifton, N.J.). 2018; 1711: 243–259. https://doi.org/10.1007/978-1-4939-7493-1_12.

[18] Giambelluca S, Ochs M, Lopez-Rodriguez E. Resting time after phorbol 12-myristate 13-acetate in THP-1 derived macrophages provides a non-biased model for the study of NLRP3 inflammasome. Frontiers in Immunology. 2022; 13: 958098. https://doi.org/10.3389/fimmu.2022.958098.

[19] Clara JA, Monge C, Yang Y, Takebe N. Targeting signalling pathways and the immune microenvironment of cancer stem cells - a clinical update. Nature Reviews. Clinical Oncology. 2020; 17: 204–232. https://doi.org/10.1038/s41571-019-0293-2.

[20] Zahari S, Syafruddin SE, Mohtar MA. Impact of the Cancer Cell Secretome in Driving Breast Cancer Progression. Cancers. 2023; 15: 2653. https://doi.org/10.3390/cancers15092653.

[21] Clendenen TV, Ge W, Koenig KL, Afanasyeva Y, Agnoli C, Bertone-Johnson E, *et al*. Breast Cancer Risk Factors and Circulating Anti-Müllerian Hormone Concentration in Healthy Premenopausal Women. The Journal of Clinical Endocrinology and Metabolism. 2021; 106: e4542–e4553. https://doi.org/10.1210/clinem/dgab461.

[22] Ding S, Sun X, Zhu L, Li Y, Chen W, Shen K. Identification of a novel immune-related prognostic signature associated with tumor microenvironment for breast cancer. International Immunopharmacology. 2021; 100: 108122. https://doi.org/10.1016/j.intimp.2021.108122.

[23] Zhou L, Rueda M, Alkhateeb A. Classification of Breast Cancer Nottingham Prognostic Index Using High-Dimensional Embedding and Residual Neural Network. Cancers. 2022; 14: 934. https://doi.org/10.3390/cancers14040934.

[24] Mehta AK, Kadel S, Townsend MG, Oliwa M, Guerriero JL. Macrophage Biology and Mechanisms of Immune Suppression in Breast Cancer. Frontiers in Immunology. 2021; 12: 643771. https://doi.org/10.3389/fimmu.2021.643771.

[25] Zhang JZ, Liu J, Xu YX, Pu WY, Shen MJ, Jiang KQ, *et al*. Identification of the mitochondrial protein ADCK2 as a therapeutic oncotarget of NSCLC. International Journal of Biological Sciences. 2022; 18: 6163–6175. https://doi.org/10.7150/ijbs.78354.

[26] Vázquez-Fonseca L, Schaefer J, Navas-Enamorado I, Santos-Ocaña C, Hernández-Camacho JD, Guerra I, *et al*. *ADCK2* Haploinsufficiency Reduces Mitochondrial Lipid Oxidation and Causes Myopathy Associated with CoQ Deficiency. Journal of Clinical Medicine. 2019; 8: 1374. https://doi.org/10.3390/jcm8091374.

[27] Jacquet N, Zhao Y. The ADCK Kinase Family: Key Regulators of Bioenergetics and Mitochondrial Function and Their Implications in Human Cancers. International Journal of Molecular Sciences. 2025; 26: 5783. https://doi.org/10.3390/ijms26125783.

[28] Brough R, Frankum JR, Sims D, Mackay A, Mendes-Pereira AM, Bajrami I, *et al*. Functional viability profiles of breast cancer. Cancer Discovery. 2011; 1: 260–273. https://doi.org/10.1158/2159-8290.CD-11-0107.